VIP The following Communications have been judged by at least two referees to be "very important papers" and will be published online at www.angewandte.org soon:

*B. L. Merner, L. N. Dawe, G. J. Bodwell**
1,1,8,8-Tetramethyl[8](2,11)teropyrenophane: Half of an Aromatic Belt and a Segment of an (8,8) Single-Walled Carbon Nanotube

*B. Liu, H. Wang, H. Xie, B. Zeng, J. Chen, J. Tao, T. B. Wen, Z. Cao, H. Xia**
Osmapyridine and Osmapyridinium from a Formal [4+2] Cycloaddition Reaction

*J. L. Alonso-Gómez, P. Rivera-Fuentes, N. Harada, N. Berova, F. Diederich**
An Enantiomerically Pure Alleno-Acetylenic Macrocycle: Synthesis and Rationalization of Its Outstanding Chiroptical Response

*P. García-García, M. A. Fernández-Rodríguez, E. Aguilar**
Gold-Catalyzed Cycloaromatization of 2,4-Dien-6-yne Carboxylic Acids: Synthesis of 2,3-Disubstituted Phenols and Unsymmetrical Bi- and Terphenyls

*H. Jiang, P. Elsner, K. L. Jensen, A. Falcicchio, V. Marcos, K. A. Jørgensen**
Achieving Molecular Complexity by Organocatalytic One-Pot Strategies: A Fast Entry for the De Novo Synthesis of Sphingoids, Amino Sugars and Polyhydroxylated α-Amino Acids

P. A. Rupar, R. Bandyopadhyay, B. F. T. Cooper, M. R. Stinchcombe, P. J. Ragogna, C. L. B. Macdonald, K. M. Baines**
Cationic Crown Ether Complexes of Germanium(II)

*T. J. Kucharski, Z. Huang, Q.-Z. Yang, Y. Tian, N. C. Rubin, C. D. Concepcion, R. Boulatov**
Kinetics of Thiol/Disulfide Exchange Correlates Weakly with the Restoring Force in the Disulfide Moiety

*W. Xu, X. Xue, T. Li, H. Zeng, X. Liu**
Ultrasensitive and Selective Colorimetric DNA Detection by Nicking Endonuclease-Assisted Nanoparticle Amplification

Author Profile

"The most exciting thing about my research is to create new molecules and new concepts. When I was eighteen I wanted to be an industrial chemist. …"
This and more about Koop Lammertsma can be found on page 4670.

Books

Highlights

Glycoproteins

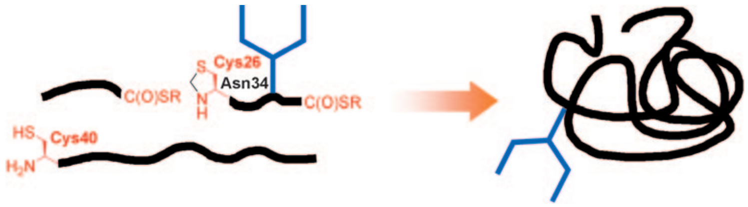

A labor of love: The synthesis of an active pure enzyme (RNase) glycoform by the native chemical ligation of a (glyco)peptide and peptide thioester fragments required numerous painstaking steps: the strategy was optimized, active inteins accessed, redox conditions fine-tuned, and glycoamino acid building blocks synthesized.

Contents

Synthetic Methods

C. Anaya de Parrodi,
P. J. Walsh* ________ **4679 – 4682**

All Kinds of Reactivity: Recent Breakthroughs in Metal-Catalyzed Alkyne Chemistry

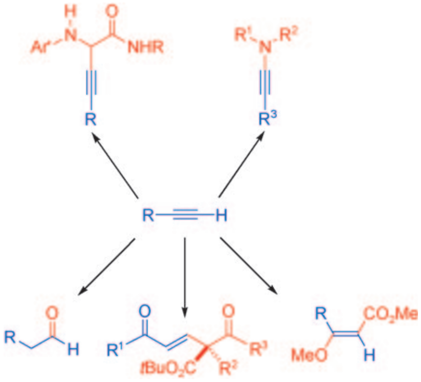

Alkynes of reactions: Recent breakthroughs in metal-catalyzed alkyne reactions, which expand the synthetic utility of alkynes, have been achieved. These approaches broaden the range of alkynes that are accessible by C—N and C—C bond-forming reactions and demonstrate that the use of bifunctional heterobimetallic catalysts can lead to new reactivity and excellent enantioselectivity (see scheme).

Genomics

J. Ibach, S. Brakmann* ____ **4683 – 4685**

Sequencing Single DNA Molecules in Real Time

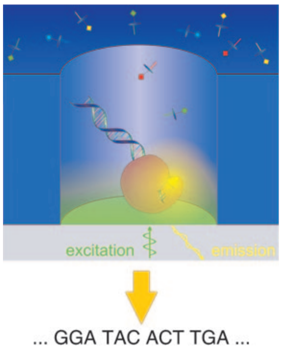

One's enough: The direct observation of a DNA-polymerase-based "sequencing engine" using single-molecule detection recently allowed single-molecule sequencing by synthesis in real time. Nucleotides with a fluorescent marker at the 5′-phosphate unit and zero-mode waveguides are crucial components of this approach, which at last promises low-cost genome-scale sequencing.

Reviews

Polyketide Biosynthesis

C. Hertweck* ________ **4688 – 4716**

The Biosynthetic Logic of Polyketide Diversity

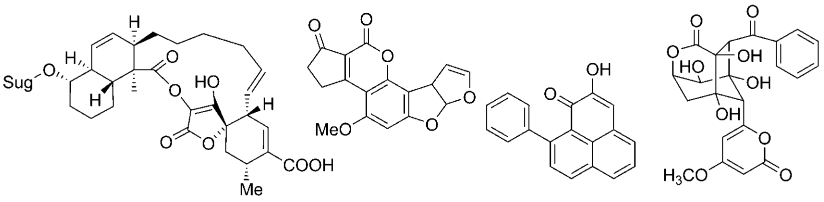

Molecular Lego: Polyketides represent a highly diverse group of natural products with structurally intriguing carbon skeletons (see picture) which are assembled from simple acyl building blocks. A combination of chemical, biochemical, and genetics studies have provided exciting new insights into the programming of polyketide assembly and the sophisticated enzymatic machineries involved. This review highlights recent developments in the field.

For the USA and Canada:
ANGEWANDTE CHEMIE International Edition (ISSN 1433-7851) is published weekly by Wiley-VCH, PO Box 191161, 69451 Weinheim, Germany. Air freight and mailing in the USA by Publications Expediting Inc., 200 Meacham Ave., Elmont, NY 11003. Periodicals postage paid at Jamaica, NY 11431. US POSTMASTER: send address changes to *Angewandte Chemie*, Wiley-VCH, 111 River Street, Hoboken, NJ 07030. Annual subscription price for institutions: US$ 7225/6568 (valid for print and electronic / print or electronic delivery); for individuals who are personal members of a national chemical society prices are available on request. Postage and handling charges included. All prices are subject to local VAT/sales tax.

Communications

Enzyme Inhibitors

W. S. Horne, C. A. Olsen, J. M. Beierle,
A. Montero, M. R. Ghadiri* **4718 – 4724**

Probing the Bioactive Conformation of an Archetypal Natural Product HDAC Inhibitor with Conformationally Homogeneous Triazole-Modified Cyclic Tetrapeptides

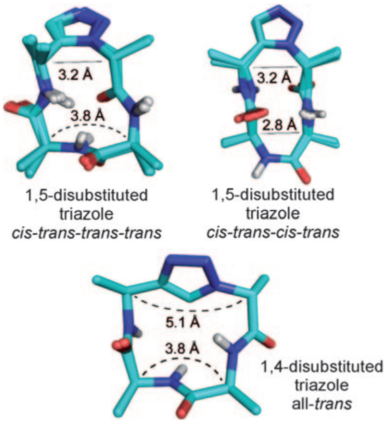

Fooling enzymes with mock amides: Analogues of apicidin, a cyclic-tetrapeptide inhibitor of histone deacetylase (HDAC), were designed with a 1,4- or 1,5-disubstituted 1,2,3-triazole in place of a backbone amide bond to fix the bond in question in either a *trans*-like or a *cis*-like configuration. Thus, the binding affinity of distinct peptide conformations (see picture) could be probed. One analogue proved in some cases to be superior to apicidin as an HDAC inhibitor.

Drug Design

J. M. Beierle, W. S. Horne,
J. H. van Maarseveen, B. Waser,
J. C. Reubi, M. R. Ghadiri* **4725 – 4729**

Conformationally Homogeneous Heterocyclic Pseudotetrapeptides as Three-Dimensional Scaffolds for Rational Drug Design: Receptor-Selective Somatostatin Analogues

A would-be amide: A 1,4-disubstituted 1,2,3-triazole was used as a surrogate for a *trans* amide bond to create a library of 16 diastereomeric pseudotetrapeptides as β-turn mimetics. High-resolution structural analysis indicated that these scaffolds adopt distinct, rigid, conformationally homogeneous β-turn-like structures (see example), some of which bind somatostatin receptor subtypes selectively, and some of which show broad-spectrum activity.

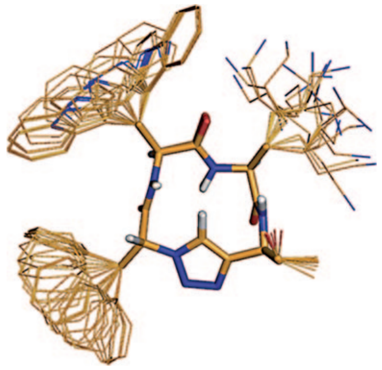

Hydrogen Storage

D. Cao, J. Lan, W. Wang,*
B. Smit* **4730 – 4733**

Lithium-Doped 3D Covalent Organic Frameworks: High-Capacity Hydrogen Storage Materials

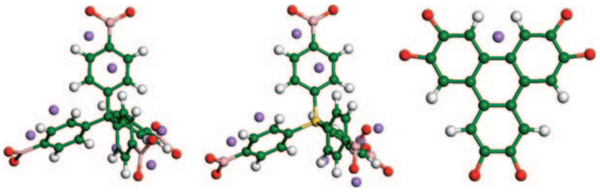

Quick on the uptake: A multiscale theoretical method predicts that the gravimetric adsorption capacities of H_2 in Li-doped covalent organic frameworks based on the building blocks shown (Li violet, H white, B pink, C green, O red, Si yellow) can reach nearly 7% at $T = 298$ K and $p = 100$ bar, suggesting that these Li-doped materials are promising adsorbents for hydrogen storage.

Ir≡N Hydrogenation

J. Schöffel, A. Y. Rogachev,
S. DeBeer George,
P. Burger* **4734 – 4738**

Isolation and Hydrogenation of a Complex with a Terminal Iridium–Nitrido Bond

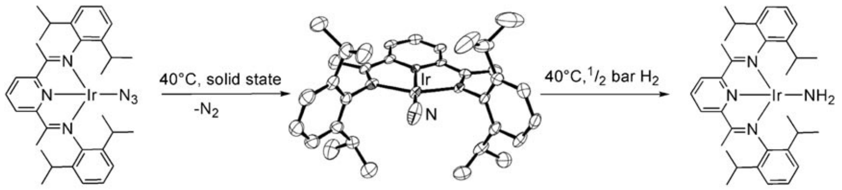

An N for Ir: The synthesis and X-ray crystal structure of a late-transition-metal complex with a terminal nitrido ligand and its hydrogenation to the related amido complex are reported (see scheme).

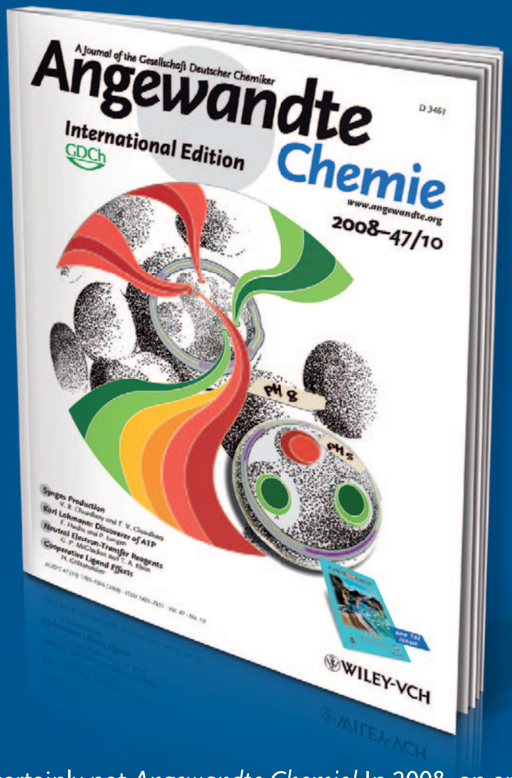
A Journal of the Gesellschaft Deutscher Chemiker
Angewandte
International Edition
GDCh
Chemie
D 3461
www.angewandte.org
2008–47/10
pH 8
pH 5
WILEY-VCH

Metal–Organic Frameworks

T. Tsuruoka, S. Furukawa, Y. Takashima, K. Yoshida, S. Isoda, S. Kitagawa* ____ **4739 – 4743**

Nanoporous Nanorods Fabricated by Coordination Modulation and Oriented Attachment Growth

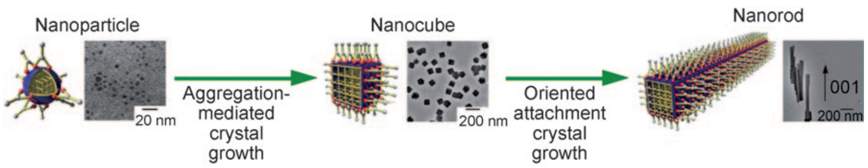

A growing attachment: Porous coordination polymer (PCP) nanorods are synthesized by modulation of the coordination equilibria between framework components, which regulates the rate of framework extension and crystal growth. Investigation of the crystal growth mechanism by TEM indicates that face-selective modulation on the surfaces of PCP crystals enhances the anisotropic crystal growth of nanorods by an oriented attachment mechanism.

Microreactors

N. Wang, T. Matsumoto, M. Ueno, H. Miyamura, S. Kobayashi* ____ **4744 – 4746**

A Gold-Immobilized Microchannel Flow Reactor for Oxidation of Alcohols with Molecular Oxygen

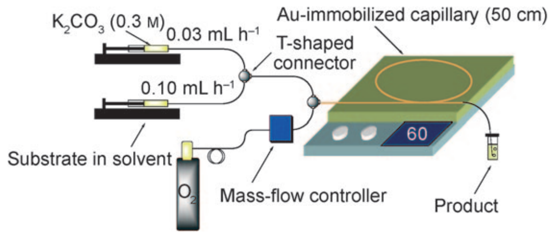

Golden capillaries: A gold-immobilized capillary column reactor allows oxidation of alcohols to carbonyl compounds using molecular oxygen. These capillary columns (see picture) can be used for at least four days without loss of activity.

Organic Nanotubes

W. Zhang, W. Jin,* T. Fukushima,* N. Ishii, T. Aida* ____ **4747 – 4750**

Metal-Ion-Coated Graphitic Nanotubes: Controlled Self-Assembly of a Pyridyl-Appended Gemini-Shaped Hexabenzocoronene Amphiphile

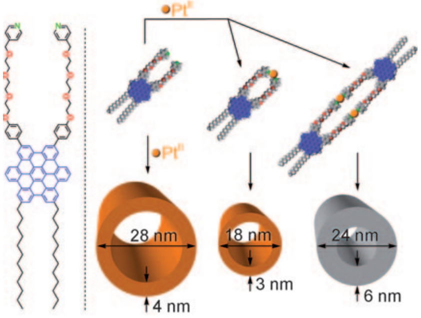

The assembly line: Hexabenzocoronene amphiphiles appended with pyridyl-terminated triethylene glycol side chains, in combination with *trans*-[$Pt(PhCN)_2Cl_2$], lead to the formation of graphitic nanotubes. The structural features and dimensions of the nanotubes depend on the assembly conditions. A platinum(II)-bridged cyclic dimer having two HBC units self-assembles into a nanotubular structure.

Electrochemistry

B. Wu, D. Hu, Y. Kuang, B. Liu, X. Zhang, J. Chen* ____ **4751 – 4754**

Functionalization of Carbon Nanotubes by an Ionic-Liquid Polymer: Dispersion of Pt and PtRu Nanoparticles on Carbon Nanotubes and Their Electrocatalytic Oxidation of Methanol

Small beginnings: Metal nanoparticle/CNT nanohybrids are synthesized from carbon nanotubes (CNTs) functionalized with an ionic-liquid polymer. The Pt and PtRu nanoparticles with narrow size distribution (average diameter: (1.3 ± 0.4) nm for PtRu, (1.9 ± 0.5) nm for Pt) are dispersed uniformly on the CNTs (see images) and show good performance in methanol electrooxidation.

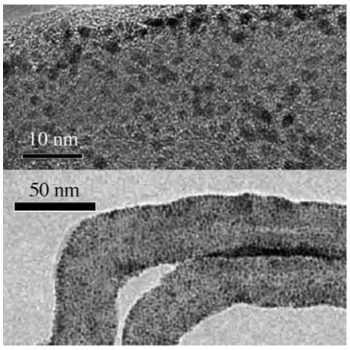

Imaging Agents

Z.-X. Jiang, X. Liu, E.-K. Jeong,
Y. B. Yu* ———— 4755 – 4758

Symmetry-Guided Design and Fluorous Synthesis of a Stable and Rapidly Excreted Imaging Tracer for ^{19}F MRI

Getting FIT: A bispherical ^{19}F imaging tracer, ^{19}FIT, was designed and synthesized. ^{19}FIT is advantageous over perfluorocarbon-based ^{19}F imaging agents, as it is not retained in the organs and does not require complex formulation procedures. Imaging agents such as ^{19}FIT can lead to ^{19}F magnetic resonance imaging (MRI) playing an important role in drug therapy, analogous to the role played by ^{1}H MRI in disease diagnosis.

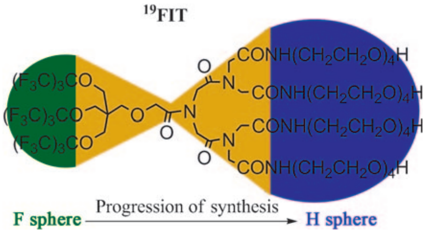

Responsive Materials

S. Liu, J. Li, Q. Shen, Y. Cao, X. Guo,*
G. Zhang, C. Feng, J. Zhang, Z. Liu,
M. L. Steigerwald, D. Xu,*
C. Nuckolls* ———— 4759 – 4762

Mirror-Image Photoswitching of Individual Single-Walled Carbon Nanotube Transistors Coated with Titanium Dioxide

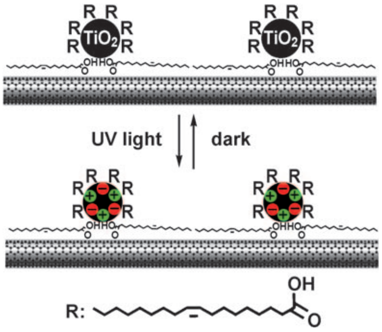

Dotting the i's: Stimuli-responsive optoelectronic devices are formed from the title transistors functionalized with photoactive quantum dots. The p-type semiconducting tubes show a fast current decrease under UV irradiation and reversibility when the UV irradiation is switched off. In contrast, ambipolar tubes show mirror-image photoswitching effects when negative and positive gate bias voltages are applied.

C_1 Chemistry

D. Preti, S. Squarcialupi,
G. Fachinetti* ———— 4763 – 4766

Aerobic, Copper-Mediated Oxidation of Alkaline Formaldehyde to Fuel-Cell Grade Hydrogen and Formate: Mechanism and Applications

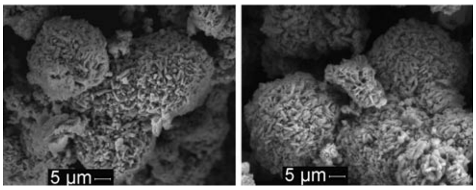

Beyond nanopowders: Hydrogen and formate are produced through the oxidation of alkaline HCHO by CuO microparticles. The Cu microparticles formed in the purely electrochemical reduction of CuO preserve the morphology of CuO (left-hand image: CuO; right-hand image: Cu formed in the reduction of CuO by alkaline HCHO) and can be permeated by a gas. They react more efficiently than Cu nanoparticles with air to restore CuO.

Functional Porous Materials

M. Ohba,* K. Yoneda, G. Agustí,
M. C. Muñoz, A. B. Gaspar, J. A. Real,*
M. Yamasaki, H. Ando, Y. Nakao,
S. Sakaki, S. Kitagawa* ———— 4767 – 4771

Bidirectional Chemo-Switching of Spin State in a Microporous Framework

The ins and outs of spin: Using the microporous coordination polymer $\{Fe(pz)[Pt(CN)_4]\}$ (**1**, pz = pyrazine), incorporating spin-crossover subunits, two-directional magnetic chemo-switching is achieved at room temperature. In situ magnetic measurements following guest vapor injection show that most guest molecules transform **1** from the low-spin (LS) state to the high-spin (HS) state, whereas CS_2 uniquely causes the reverse HS-to-LS transition.

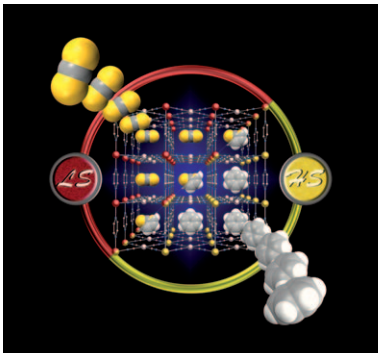

Biomimetic Synthesis

S. Kang, C. C. Jolley, L. O. Liepold,
M. Young,* T. Douglas* ___ 4772 – 4776

From Metal Binding to Nanoparticle Formation: Monitoring Biomimetic Iron Oxide Synthesis within Protein Cages using Mass Spectrometry

Mass measurements of metal-mineralized protein cages allowed quantitative examination of the effects of metal-ion concentration on the final nanoparticle size. Modeling using a kinetic master equation suggests that particle growth involves both a binding phase and a growth phase (see picture; I: relative abundance; LiDps: a DNA binding protein; ^{n}Fe: number of Fe atoms).

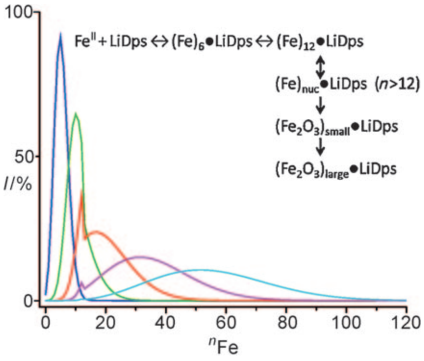

Thin Films

Y. Liu, C. M. Lew, M. Sun, R. Cai, J. Wang,*
G. Kloster, B. Boyanov,
Y. Yan* ___ 4777 – 4780

On-Wafer Crystallization of Ultralow-κ Pure Silica Zeolite Films

A higher goal: An on-wafer crystallization process to prepare pure silica zeolite (PSZ) MEL-type films that is superior to the previously used hydrothermal process is reported. These striation-free MEL-type films (right, see picture) outperform the traditional spin-on films (left) in terms of the κ value, mechanical properties, surface roughness, mesopore size, and size distribution.

Anion Template

K. M. Mullen, J. Mercurio, C. J. Serpell,
P. D. Beer* ___ 4781 – 4784

Exploiting the 1,2,3-Triazolium Motif in Anion-Templated Formation of a Bromide-Selective Rotaxane Host Assembly

Bromide is best: The first [2]rotaxane incorporating the triazolium anion-binding motif is prepared using bromide anion template. Preliminary anion-binding investigations reveal that the rotaxane exhibits the rare selectivity preference for bromide over chloride ions.

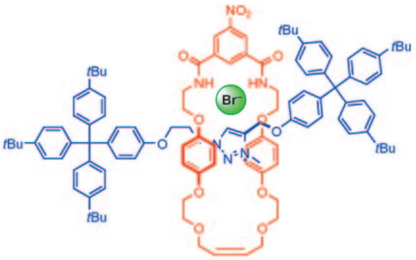

Biosensors

C.-H. Lu, H.-H. Yang,* C.-L. Zhu, X. Chen,
G.-N. Chen ___ 4785 – 4787

A Graphene Platform for Sensing Biomolecules

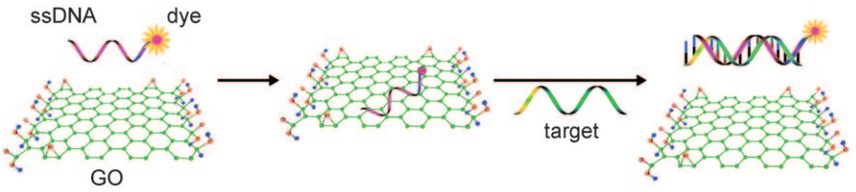

Sensitive platform: The use of graphene oxide (GO) as a platform for the sensitive and selective detection of DNA and proteins is presented. The interaction of GO and dye-labeled single-stranded DNA leads to quenching of the dye fluorescence. Conversely, the presence of a target DNA or protein leads to the binding of the dye-labeled DNA and target, releasing the DNA from GO, thereby restoring the dye fluorescence (see picture).

Nanoparticles

M. Bremholm, M. Felicissimo,
B. B. Iversen* ____________ 4788 – 4791

Time-Resolved In Situ Synchrotron X-ray Study and Large-Scale Production of Magnetite Nanoparticles in Supercritical Water

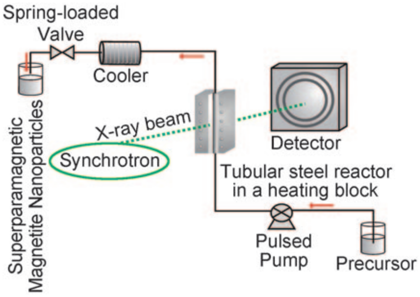

A general solution: In situ synchrotron X-ray scattering in a high-pressure pulsed injection reactor (see picture) shows that magnetite nucleation and growth are temporally separated. Gram-scale crystalline, pure phase, superparamagnetic magnetite nanoparticles were synthesized without surfactants in supercritical water in less than one hour using a laboratory-scale continuous-flow reactor.

Bent Allenes

M. Melaimi, P. Parameswaran,
B. Donnadieu, G. Frenking,*
G. Bertrand* ____________ 4792 – 4795

Synthesis and Ligand Properties of a Persistent, All-Carbon Four-Membered-Ring Allene

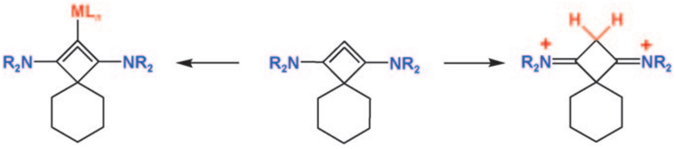

A single donor substituent at each terminus is sufficient to make the CCC skeleton of allenes very flexible and give carbon(0) character to the central carbon atom. This allows the synthesis of a four-membered carbocyclic allene, which can be doubly protonated and behaves as a very strong η^1-donor ligand for transition metals (see scheme).

Unsaturated Carbenes

M. Asay, B. Donnadieu, W. W. Schoeller,
G. Bertrand* ____________ 4796 – 4799

Synthesis of Allenylidene Lithium and Silver Complexes, and Subsequent Transmetalation Reactions

Alpha, beta, gamma! Amino substituents in alpha and beta positions allow the isolation of free carbenes, but even in the gamma position, their strong π-electron-donating properties permit the synthesis of allenylidene lithium adducts and silver complexes (see picture), which are ideal precursors for the preparation of various transition-metal–allenylidene complexes.

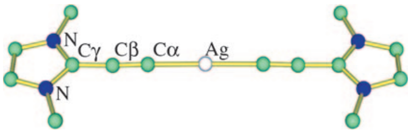

HCOOH Dehydrogenation on Au

M. Ojeda, E. Iglesia* ______ 4800 – 4803

Formic Acid Dehydrogenation on Au-Based Catalysts at Near-Ambient Temperatures

Selective HCOOH decomposition to H_2/CO_2 on Au: Au species catalyze HCOOH dehydrogenation at higher rates than on Pt, previously considered the most active metal. Dehydrogenation occurs through formate decomposition limited by H_2 desorption on Au species undetectable by TEM. CO did not form (< 10 ppm), making products suitable for low-temperature fuel cells.

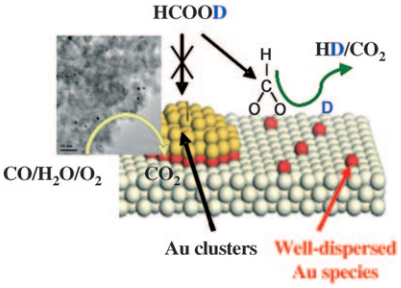

Radicals

A. Mardyukov, E. Sanchez-Garcia,
R. Crespo-Otero,
W. Sander* ____________ 4804 – 4807

Interaction and Reaction of the Phenyl Radical with Water: A Source of OH Radicals

That's radical! A photochemical reaction between the phenyl radical and water results in the abstraction of a hydrogen atom from water and the formation of a hydroxyl radical. The hydroxyl radical forms an OH⋯π hydrogen bond with benzene (see picture) and does not react with benzene thermally under the conditions of matrix isolation.

Nanostructures

X. Q. Huang, H. H. Zhang, C. Y. Guo, Z. Y. Zhou, N. F. Zheng* ___ **4808–4812**

Simplifying the Creation of Hollow Metallic Nanostructures: One-Pot Synthesis of Hollow Palladium/Platinum Single-Crystalline Nanocubes

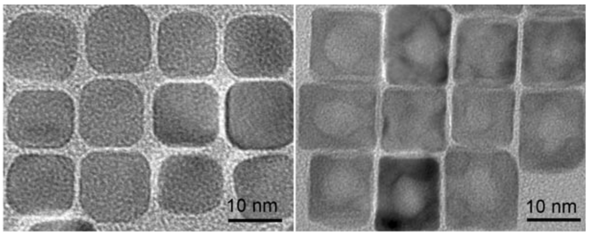

Efficiency simplified: A synthetic strategy has been developed to prepare single-crystalline hollow Pd/Pt nanocubes (right, see picture; left: nanocubes). Compared to the solid Pd/Pt nanocubes of similar sizes, the hollow Pd/Pt nanocubes increase accessible surface area and therefore improve electrocatalytic activity in formic acid oxidation.

Carbonylation

F. E. Celik, T. J. Kim, A. T. Bell* ___ **4813–4815**

Vapor-Phase Carbonylation of Dimethoxymethane over H-Faujasite

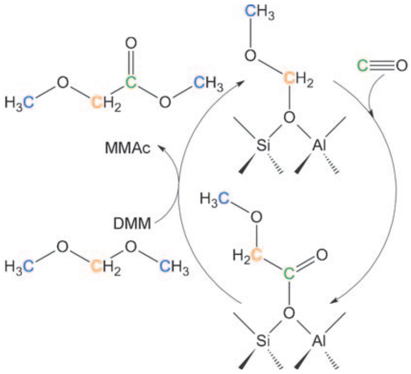

Carbonylation gets a phase lift: The usual liquid-phase, high-pressure processes for carbonylating formaldehydes are avoided in a novel vapor-phase reaction. Using an acid zeolite (Faujasite) at near-atmospheric pressure dimethoxymethane (DMM; the dimethyl acetal of formaldehyde; see scheme) is carbonylated to produce methyl methoxyacetate (MMAc). This approach provides a new route to ethylene glycol under mild conditions.

Self-Assembly

C. Chen, W. Chen, J. Lu, D. Chu, Z. Huo, Q. Peng, Y. Li* ___ **4816–4819**

Transition-Metal Phosphate Colloidal Spheres

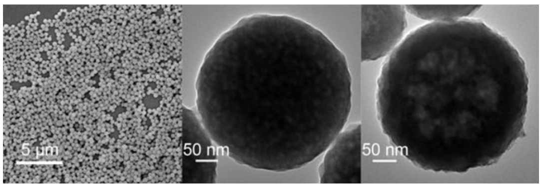

The music of the spheres: Transition-metal phosphate colloidal spheres with one metal (Mn, Fe, Co, Ni, and Cu; see picture) or more than one metal (such as Fe–Ni, Co–Cu, Fe–Co–Cu, Fe–Co–Ni–Cu, Mn–Fe–Co–Ni–Cu, and Mn–Fe–Co–Ni–Cu–Zn) were synthesized in solution at low temperature. Porous and hollow iron phosphate spheres were prepared by adjusting the pH value of the reaction.

Nanotechnology

J. Ryu, C. B. Park* ___ **4820–4823**

Synthesis of Diphenylalanine/Polyaniline Core/Shell Conducting Nanowires by Peptide Self-Assembly

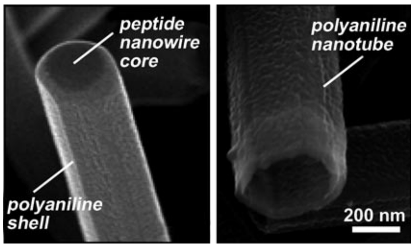

Breaking the mold: Self-assembled peptide nanowires were used as a template for the synthesis of hollow polyaniline (PANI) nanotubes (see scanning electron microscopy images). The thickness and the morphology of the PANI nanostructures could be controlled readily either by varying the reaction time or by applying multiple PANI coatings.

Contents

Nanostructures

C. M. Cobley, M. Rycenga, F. Zhou, Z.-Y. Li, Y. Xia* ______ **4824 – 4827**

Etching and Growth: An Intertwined Pathway to Silver Nanocrystals with Exotic Shapes

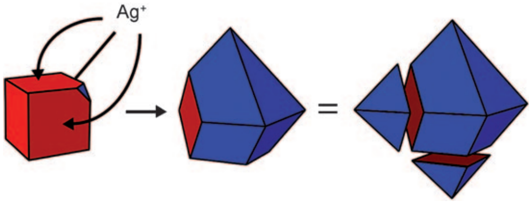

Two-faced nanocrystals: Rapid addition of a second aliquot of silver nitrate during a polyol synthesis led to the formation of anisotropically truncated octahedrons as a result of oxidative etching and overgrowth of silver nanocubes. Three adjacent faces of the nanocube grew more rapidly than the three other faces, generating a non-centrosymmetric structure (see picture).

Monomeric Phosphazenes

X. Zeng, H. Beckers, H. Willner* ______ **4828 – 4831**

Difluoro-λ⁵-Phosphinonitrile $F_2P{\equiv}N$: Matrix Isolation and Photoisomerization into FP=NF

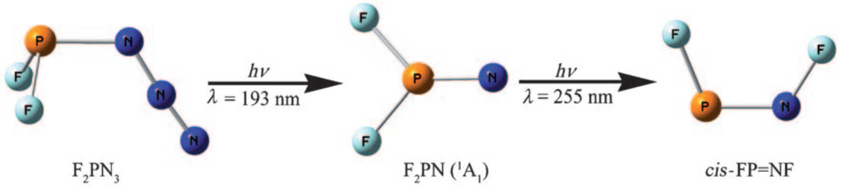

Splendid isolation: Monomeric phosphazene F_2PN ($^1A_1$) was prepared for the first time through irradiation of F_2PN_3 in an argon matrix with an ArF excimer laser ($\lambda = 193$ nm). Upon subsequent irradiation with a high-pressure mercury arc lamp ($\lambda = 255$ nm), F_2PN undergoes a 1,2-fluorine shift to give iminophosphane *cis*-FP=NF.

Reactive Intermediates

R. S. Grainger,* B. Patel, B. M. Kariuki ______ **4832 – 4835**

2,7-Di-*tert*-butylnaphtho[1,8-*cd*]-[1,2]dithiole 1,2-dioxides: Thermally Stable, Photochemically Active *vic*-Disulfoxides

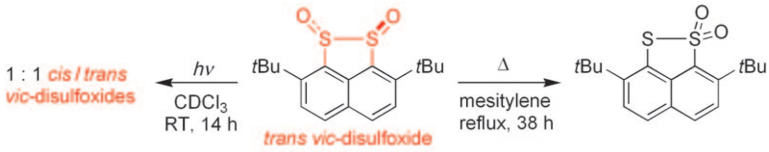

Bulking up: The thermal barrier to rearrangement of a *vic*-disulfoxide is significantly increased through steric buttressing about the (O)S–S(O) bond. Whereas the title compounds represent the most thermally stable *vic*-disulfoxides known to date, they also undergo a novel photomediated epimerization at room temperature (see scheme).

Hydrocarbon Chemistry

A. D. Payne, G. Bojase, M. N. Paddon-Row,* M. S. Sherburn* ______ **4836 – 4839**

Practical Synthesis of the Dendralene Family Reveals Alternation in Behavior

Back from obscurity: The practical synthesis of the first six members of the fundamental class of acyclic branched oligoalkenes has been achieved. The syntheses allow access to the target compounds on multigram scales in good yields. Members of the family with even numbers of double bonds are significantly more stable than those with odd numbers (see picture), and exhibit different chemical reactivities in Diels–Alder reactions.

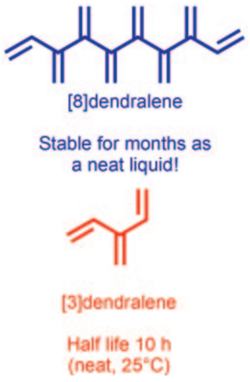

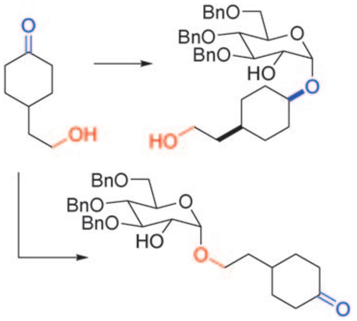

Gettin' a little sugar—no alcohol required: A procedure for the direct glycosylation of ketones without a hydroxy intermediate enables the site-selective glycosylation of hydroxyketones at the ketone or the alcohol functionality without the use of protecting groups on the aglycone (see scheme). Site selectivity is controlled by the catalyst structure in hydrosilylation and dehydrogenative silylation reactions with sugar silanes. Bn = benzyl.

Synthetic Methods

Z. A. Buchan, S. J. Bader,
J. Montgomery* ________ **4840 – 4844**

Ketone Hydrosilylation with Sugar Silanes Followed by Intramolecular Aglycone Delivery: An Orthogonal Glycosylation Strategy

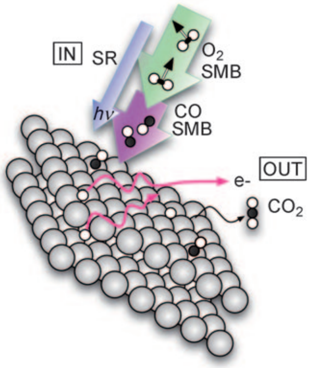

Sticking together: The occupation of different sites by oxygen atoms that are produced by the dissociation of O_2 on Pd(100) is determined by the initial rotational alignment of the parent molecules. The atom locations are characterized by different chemical reactivities in the reaction with CO to form CO_2 (see picture), which are followed by synchrotron radiation (SR) experiments with a supersonic molecular beam (SMB).

Chemisorption

L. Vattuone,* A. Gerbi, D. Cappelletti,
F. Pirani, R. Gunnella, L. Savio,
M. Rocca ________ **4845 – 4848**

Selective Production of Reactive and Nonreactive Oxygen Atoms on Pd(001) by Rotationally Aligned Oxygen Molecules

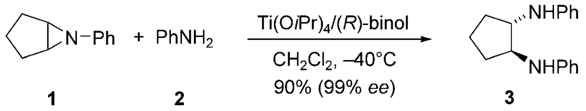

It's as simple as that: An in situ prepared chiral catalyst from the commercially available compounds Ti(O*i*Pr)$_4$ and (*R*)-binol catalyzes the highly enantioselective ring-opening of *meso*-aziridines **1** with anilines **2** and furnishes valuable chiral 1,2-diamines **3** in high yields and up to 99% *ee*. (*R*)-binol = (*R*)-2,2′-dihydroxy-1,1′-binaphthyl.

Asymmetric Catalysis

S. Peruncheralathan, H. Teller,
C. Schneider* ________ **4849 – 4852**

Titanium Binolate Catalyzed Aminolysis of *meso* Aziridines: A Highly Enantioselective and Direct Access to 1,2-Diamines

The attachment of modulators to a trimeric porin ion channel was investigated (see picture of the trimer with a crown ether modulator (orange)). The interplay of modulator and protein is essential for the conformational heterogeneity of the hybrid channel. Single-site attachment in large pores is not sufficient to change the electrophysiological characteristics of the pores—such change requires additional noncovalent interactions or second-site attachments.

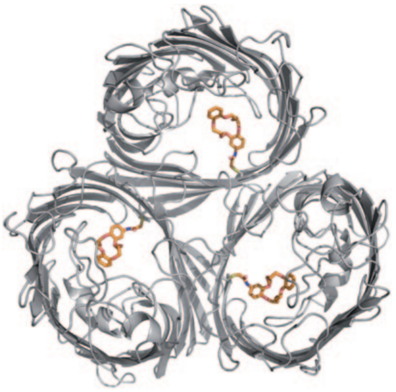

Ion Channels

S. Reitz, M. Cebi, P. Reiß, G. Studnik,
U. Linne, U. Koert,*
L.-O. Essen* ________ **4853 – 4857**

On the Function and Structure of Synthetically Modified Porins

Contents

Inclusion Bodies

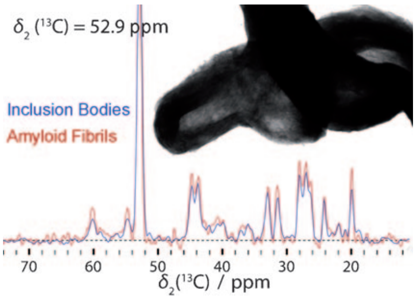

Protein deposition frequently occurs as inclusion bodies (IBs) during heterologous protein expression in *E. coli*. The structure of these *E. coli* IBs of the prion-forming domain from the fungal prion HET-s is the same as that previously determined for fibrils assembled in vitro, and show prion infectivity. These results demonstrate that the IBs of HET-s(218–289) are amyloids.

Oxygen-Centered Radicals

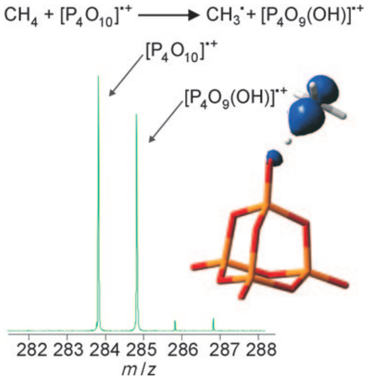

No need for a metal: A combination of mass spectrometry and computational studies (density functional theory and coupled-cluster methods) shows that $[P_4O_{10}]^{\bullet+}$ is the first polynuclear nonmetal oxide cation that is capable of activating the C—H bond of methane at room temperature (see picture). This process represents a further example in the reactivity of oxygen-centered radicals.

Supporting information is available on www.angewandte.org (see article for access details).

A video clip is available as Supporting Information on www.angewandte.org (see article for access details).

Service